Composite Structures 212 (2019) 524–534

Contents lists available at ScienceDirect

Composite Structures

journal homepage: www.elsevier.com/locate/compstruct

Lower stiffness of GFRP after sulfuric acid-solution aging is due to degradation of fibre-matrix interfaces?

M. Kanerva[a,*], J. Jokinen[a], E. Sarlin[a], T. Pärnänen[a,b], M. Lindgren[c], M. Järventausta[a], J. Vuorinen[a]

[a] Tampere University of Technology, Laboratory of Materials Science, P.O. Box 589, FI-33101 Tampere, Finland
[b] Aalto University, School of Engineering, Department of Mechanical Engineering, P.O. Box 14300, FI-00076 Aalto, Finland
[c] Outotec Research Center, P.O. Box 69, 28101 Pori, Finland

ARTICLE INFO

Keywords:
Aging
Finite element modelling
GFRP
Sulfuric acid
Elasticity

ABSTRACT

The aging effects on composite stiffness are important when structures are monitored under long-term mechanical loads and harsh chemical environment. This work aims to reveal the role of fibre-to-matrix interfacial aging on elastic constants due to a long-term sulfuric acid immersion at a high temperature and pressure. The aging effects of glass fibre matrix interfaces are rather impossible to measure directly and they cannot be easily subtracted from macro scale test results. Here, extensive numerical simulations are automatically run to show the sensitivity of all the essential elastic constants on the experimentally observed output of mechanical tests in reality. Material models are formulated for two different length-scales to understand (1) the sensitivity of the layer's length scale related elastic constants and (2) micro scale material properties. The well-established Halpin-Tsai parameters are used to include interfacial effects. The experimental results show that the aging significantly affects tensile and flexural behavior of glass fibre vinylester epoxy composites: tensile and flexural stiffness decreased 6–49% and ultimate strength values 13–34%. The simulations presented that the degradation of fibre matrix interfaces cannot be excluded and they verified the degradation of glass-fibres' modulus due the conditioning.

1. Introduction

Besides the fact that polymer composites have proven to be superior materials for lightweight applications and integral structures with a minimum amount of fasteners, composites are an excellent selection for pipes and containers for hazardous substances. Containers and process reactors for alkaline and acidic process fluids are typically made of glass fibre-reinforced plastics (GFRPs) in order to realize a product at a reasonable costs and necessary durability. However, due to the complexity of aging mechanisms in GFRP when it is subjected to aqueous solutions, the operational life time and ultimate failure still are difficult to predict accurately [1,2]. Improved predictions of the changes in stiffness because of aging would prevent casualties and financial losses throughout the industry sector.

A significant effort has been made on the creation of damage models of advanced composites during the last two decades. Damage in all its varied modes, three dimensional loading, and different laminate configurations remain an issue under intensive research work for composites. Even when the work to solve damage modelling at ambient laboratory conditions is on-going, the investigation of composite materials' aging in harsh environments and related damage models must progress alongside. The state-of-art continuum aging modelling, in the current literature, has been devoted either to:

- the formulation of progress of degradation as a function of time, or, to
- the distinguishing of separate effects of fibre, matrix and interface on aging or diffusion of fluids causing the degradation.

The well-known laminate constants and hygro-thermal properties [3] are typically the foundation of the reported aging models, e.g. in the ones that use exponential scaling factors to fit the aging according to experimental data [4]. Oliveira and Creus [5] reviewed the known aging mechanisms in detail and formulated a non-linear viscoelastic model with a creep compliance function to account for aging as a function of time in a general composite layer and run several examples on a finite element basis. However, the degradation in their model is given via state variables, which do not consider a physically understandable material property or distinguish different intralayer aging mechanisms, not to mention effects originating from layer interfaces.

* Corresponding author.
E-mail address: Mikko.Kanerva@tut.fi (M. Kanerva).

https://doi.org/10.1016/j.compstruct.2019.01.006
Received 31 August 2018; Received in revised form 9 November 2018; Accepted 2 January 2019
Available online 04 January 2019

The interfaces between reinforcement layers with different orientation also influence the laminate aging. The type of the aging in the layer interface depends on the bond preparation meaning the lamination technique and addition of tough polymer phases [6,7].

For carbon fibre-reinforced plastics, the aging of fibres is typically neglected. In turn, the degradation of bare E (ECR) glass-fibres subjected to acidic solutions or other harsh environments has been clearly demonstrated [8,9]. In the case of a composite, the strength of a fibre in a bundle embedded by the matrix is rather impossible to test, and so has the effect of fibre aging on laminate properties left unresolved in the current literature. The matrix polymer in carbon-fibre or glass fibre-reinforced composites is affected by elevated temperatures as well as by any aqueous-acidic fluid absorption. However, the behavior of cross-linked matrices is biased since short-term exposure might not actually deteriorate the polymer network but enhance it via post-cure reactions and, hence, improve the composite's matrix-governed properties [10,11].

The work at hand aims to understand and quantify the effect of fibre aging on the stiffness degradation of GFRP composites subjected to conditioning in sulfuric acid solution (90 °C, 15 bar pressure [12]). The changes in the laminate stiffness and the resulting deformations under static loading can be used to monitor the status and predict probable failure due to aging of a full-scale composite structure. The preceding work has shown that the aging leads to deterioration of ultimate strength and the proof stress limit in thick laminates [13] where the differentiation of separate aging mechanisms could not be demonstrated. Therefore, the first part of this study covers tensile and flexural tests for the matrix and two different laminate lay-ups to reveal aging behavior that is governed by either matrix, fibre or fibre matrix-related interfaces. In the second part of the study, we automatize the execution of looped numerical simulations (see reported applications, e.g. [14,15]) to screen the sensitivity of stiffness to particular aging mechanisms. The material modelling is carried out on two different length scales to trace the essential properties causing observed changes to a test response. Finally, the potential interfacial degradation is studied by fitting the interfacial Halpin-Tsai parameters for the applied GFRP in the aged condition.

2. Material and methods

2.1. Experiments

2.1.1. Laminate and matrix sample preparation

GFRP laminates were fabricated using ECR glass-fibre yarn (E6CR17-2400-386T, 14A, JS/004-2JC-54, Jushi) and roving tape (E-T450, 230 mm) as reinforcement, and epoxy-vinylester resin (Derakane 441, Ashland Composites; ME-50 LA, Peroxan) as matrix. A rotating mandrel with a square cross-section was used to filament-wind four flat laminates at a time. Two different series were wound using lay-ups of $[0^\circ_4/90^\circ/0^\circ/90^\circ/0^\circ_4]$ and $[0^\circ_3/90^\circ_4/0^\circ_3]$ (termed here as lay-up 1 and lay-up 2, respectively), where each 0° layer contains 560 g/m^2 of continuous winding yarn and each 90° layer 450 g/m^2 of roving. Dry reinforcement was wound and the resin was infused after vacuum bagging the mandrel. The laminates were post-cured for 10 h at 80 °C. Nominal thickness of a cured laminates was 4 mm. In addition to the laminates, pure matrix resin samples with nominal 6 mm thickness were cast on aluminum molds (20 cm × 20 cm).

2.1.2. Conditioning

The cut-off flat laminates (30 cm × 15 cm) were sealed at edges using the matrix resin and individually weighed before the conditioning. GFRP reactors were used to submerge the laminates and matrix samples into sulfuric acid (SAC) medium (50 g/l H_2SO_4 solution with water) at an elevated temperature and pressure (90 °C, 15 bar pressure). In addition, 0.5 g/l of $Fe_2(SO_4)_3$ was added to hinder the corrosion in the metallic parts of the conditioning system. More details of the reactor used can be found in previous studies [13,12]. The laminates were conditioned for six months and the resin samples for one year to observe degradation originating from aging.

2.1.3. Matrix three-point bending

Three-point bending tests were carried out according to ISO 178:2010. The specimens were cut using a circular saw and polished to planar dimensions of 15 mm × 80 mm. The tests were performed using a testing machine (Electropuls E 3000, Instron) with a 3 kN load cell and computerized control (WaveMatrix, Instron) using a constant displacement rate of 2 mm/min and pre-force of $F_{pr} = -15$ N. The average flexural modulus, proof stress at 0.05% plastic strain, and ultimate strength were determined. All the samples were post-cured and dried in a vacuum oven for three days (50 °C, −0.5 bar vacuum) before testing. Six virgin and six one-year conditioned samples were tested. The flexural (longitudinal) stress (σ_{fl}) was calculated using the following equation:

$$\sigma_{fl} = 3(-F)L_{sp}/(2w{\cdot}t^2), \tag{1}$$

where F is the test machine force output, L_{sp} is the loading nose span, w is the specimen width, and t is the specimen thickness. The flexural (longitudinal) strain (ε_{fl}) was in turn calculated using the following equation:

$$\varepsilon_{fl} = 6(-d){\cdot}t/L_{sp}^2, \tag{2}$$

where d is the test machine displacement output. Stress–strain curves were plotted for each specimen individually and the average flexural modulus, proof stress, and strength were calculated and provided with the standard deviations per series.

2.1.4. Tensile tests

Tensile test specimens were prepared according to ISO 527–5 using glass fibre-reinforced epoxy tabs and planar specimen shape of 250 mm × 20 mm. A hydraulic tester (Dartec, 100 kN cell) with a computerized control (Elite Suite, MTS) was used at a constant displacement rate of 1.0 mm/min. An extensometer (MTS) with a gauge length of 25 mm was fixed to the specimen gauge section to record the axial strain. The average Young's modulus (0…0.2% strain range fit), proof stress at 0.05% nonlinear strain, and ultimate strength based on the first ply failure (FPF), or the first failure by detachment of extensometer, were determined. All the specimens were dried in a vacuum oven until no mass change occurred. Three specimens were prepared for both lay-ups from virgin and six month-conditioned laminates. The engineering tensile stress (σ_{eng}) was calculated using the following equation:

$$\sigma_{eng} = F/(w_t{\cdot}t_t), \tag{3}$$

where w_t and t_t refer to the average (of three measurement points) width and thickness, respectively, of the tensile test specimen. Stress–strain curves were plotted for each specimen individually and the average modulus, proof stress, and strength were calculated and provided with the standard deviations per series.

2.1.5. ILSS tests

Interlaminar shear strength (ILSS) tests were carried out according to ASTM D2344. Specimens with a planar shape of 26 mm × 10 mm were cut out and polished into exact dimensions. The same hydraulic tester as for the tensile tests was used at a constant displacement rate of 1.0 mm/min and a loading nose separation of 18 mm. All the specimens were dried in a vacuum oven (50 °C) till no mass change occurred (details were reported previously [16]). Six specimens were tested from conditioned and virgin laminates, and also for both lay-ups. ILSS shear strength values according to the standard were calculated and are given in a report [16]. However, shear stress according to the calculation per standard does not represent proper shear stress for a non-unidirectional laminate, and is not used in this study. Here, the test data was used to calculate flexural (longitudinal) stress (σ_{fl}) and flexural (longitudinal) strain (ε_{fl}) using Eqs. (1) and (2), respectively, meaning that the maximum tensile values (peak values) in the specimen were estimated. These values refer to in-plane stress and strain in the ILSS specimen and

are outer layer-wise comparable to the tensile test (Section 2.1.4) load direction, i.e. when considering the outer (unidirectional) layer of the ILSS specimen. Stress–strain curves were plotted for each specimen individually and the average flexural modulus and strength were calculated and provided with the standard deviations per series. The flexural modulus was defined by a linear fit over the 2.0…3.5 ± 0.5% flexural strain range.

2.1.6. Characterization

The fibre volume fraction (V_f) of the composite material was determined using burn-off tests. Laminate samples (25.4 mm × 20 mm) were extracted after tensile testing from the virgin laminate specimens and aged specimens. The tests resulted in total reinforcement weight (w_f) and the volume fraction was determined using the following formula:

$$V_f = \frac{1}{1 + (\rho_f/\rho_m)(w_{tot}/w_f - 1)}, \tag{4}$$

where w_{tot} is the total sample weight, and ρ_f and ρ_m are densities of fibre and matrix, respectively. The samples were stabilised before the tests for a minimum of 40 h (20 ± 2 °C, 65 ± 4% RH). The heating was carried out in two steps (0–280 °C, in 60 min; 280–565 °C and hold for 60 min). Fibre density of $\rho_f = 2.6\ \mathrm{g/cm^3}$ and matrix density of $\rho_m = 1.16\ \mathrm{g/cm^3}$ [17] were used for calculation.

The micro scale failure modes in the tested ILSS samples were analyzed with field-emission scanning electron microscopy (FESEM) using an ULTRAplus microscope (Zeiss). The samples were embedded into epoxy blocks, polished, and coated by a thin carbon layer.

2.2. Finite element models and simulation routines

The tensile and ILSS tests were modelled using *Abaqus*® 2017 (Simulia). Full 3D models of both types of test specimens and for both lay-ups were created. The dimensions of the tensile specimen model were 250 mm × 19.86 mm and the ILSS specimen model 26 mm × 10 mm. The tabs of the tensile specimen were modelled as glass fibre-reinforced epoxy with a lay-up $[45^\circ_4/-45^\circ]$ (see Table 1) and connected using a tie constraint. The tensile specimen's tabs were restricted to move in specimen width and thickness directions. The loading was applied by an enforced displacement to the upper tabs (1.5 mm) while the axial movement of the lower tabs was restricted. The ILSS specimen was supported by two half-cylindrical pins (radius 1.6 mm, separation 18 mm) and loaded by a central pin (radius 3.15 mm); all pins were modelled as linear elastic steel. The support pins were restricted from moving and the loading was applied by an enforced displacement subjected to the loading pin (0.25 mm) with horizontal movement restricted. The layers and the loading pins were meshed using linear bricks (C3D8/ C3D8R). For each layer, an element plane was meshed so that the laminates were modelled by 11 and 10 elements in the thickness direction (Fig. 1a).

Equal layer thicknesses (i.e., nominal thicknesses divided by the number of layers) were scaled based on the measured fibre volume fraction and areal weight per reinforcement type (see Section 2.1.1), giving values of 0.363 mm and 0.292 mm for the axial and transverse layer, respectively. Hence, exact laminate thickness values of 3.851 mm and 3.346 mm were used for lay-up 1 and lay-up 2, respectively.

Table 1
Engineering constants applied for layer modelling (virgin laminate values). The GFRP layer represents a unidirectionally reinforced layer and the tab laminate ± 45° fabric-reinforced layer.

Engineering constant	GFRP layer	Tab
E_1	45 GPa	24 GPa
E_2	10 GPa	24 GPa
E_3	10 GPa	9 GPa
G_{12}	5 GPa	3.6 GPa
G_{13}	5 GPa	3.5 GPa
G_{23}	3.85 GPa	3.5 GPa
ν_{12}	0.3	0.11
ν_{13}, ν_{23}	0.3	0.3

The numerical aging analysis was carried out by applying material modelling on two different length scales. A process-integration and optimization tool Isight® (Simulia) was used to run and synchronize the simulation routines. The alteration of the elastic constants—caused by aging in the real specimens—was automatized (range 0… − 50% change per layer constant and ± 25% for fibre and matrix constants) as well as the collective, statistical analysis of the results. For surveying the influence of changes in the layer properties as well as in the micromechanics, 200 simulations were processed per test specimen type, lay-up, and length scale. In detail, a three-step process was used and it involved the input of mapped and altered input parameters for Abaqus by Isight (1), actual finite element (FE) solution per test specimen and lay-up type (2), and the post-processing of the simulation results by Isight (3), see illustration in Fig. 1b. (Optimum) Latin Hypercube Sampling (LHS) method was used for defining the essential combinations of varied material properties (more about sampling convergence in a report [15]). The target response in the FE simulations was stiffness and, given that constant enforced displacement was input, the required reaction force was recorded. A regression analysis was performed to analyse the sensitivity per material constant; Linear term Correlation Factor (LCF) was determined for each variable to resemble its potential to cause the degradation observed experimentally. Finally, an additional fitting routine was implemented for the potential impact of Halpin-Tsai parameters (see Section 2.2.3).

2.2.1. Layer modelling

For a layer's length scale, each layer was presumed linear, anisotropic continuum with nine practically independent engineering constants forming the following stress–strain model of the linear elastic regime:

$$\boldsymbol{\sigma} = \boldsymbol{D}^{el}\boldsymbol{\varepsilon}^{el}, \tag{5}$$

where

$$inv(\boldsymbol{D}^{el}) = \begin{bmatrix} 1/E_1 & -\nu_{21}/E_2 & -\nu_{31}/E_3 & 0 & 0 & 0 \\ -\nu_{12}/E_1 & 1/E_2 & -\nu_{32}/E_3 & 0 & 0 & 0 \\ -\nu_{13}/E_1 & -\nu_{23}/E_2 & 1/E_3 & 0 & 0 & 0 \\ 0 & 0 & 0 & 1/G_{12} & 0 & 0 \\ 0 & 0 & 0 & 0 & 1/G_{13} & 0 \\ 0 & 0 & 0 & 0 & 0 & 1/G_{23} \end{bmatrix}, \tag{6}$$

and $\boldsymbol{\sigma}$ is the Cauchy stress tensor and $\boldsymbol{\varepsilon}^{el}$ the tensor for (finite) strains (elastic regime). The consideration of the Poisson effect and related volume change leads to the relation $\nu_{ij}/E_i = \nu_{ji}/E_j$; basically numerical and theoretical limits can be given according to rational material behavior and stability of the computation. The baseline material property values of the engineering constants (virgin material values) are shown in Table 1. The validity of the models was studied via comparisons of force–displacement plots. The validity was confirmed for the stiffness along the linear portion of the specimen behavior, as illustrated in Section 3.4 later on.

2.2.2. Micromechanics modelling

For the analysis on the micro length scale, the reinforcement and matrix were modelled separately and the conversion into layer's elastic constants was done by using Microsoft® Excel script and by applying an additional process step to the Isight driven routine (Fig. 1b). As a starting point, the GFRP laminate was modeled as a system of fibres and matrix, with fibres having a virgin axial Young's modulus of 79.79 GPa [18], Poisson's ratio of 0.2 [19], and matrix having a virgin Young's modulus of 3.3 GPa [17] and Poisson's ratio of 0.38 [19]. Also, a constant V_f was used (being average of the measured values, 59.2%).

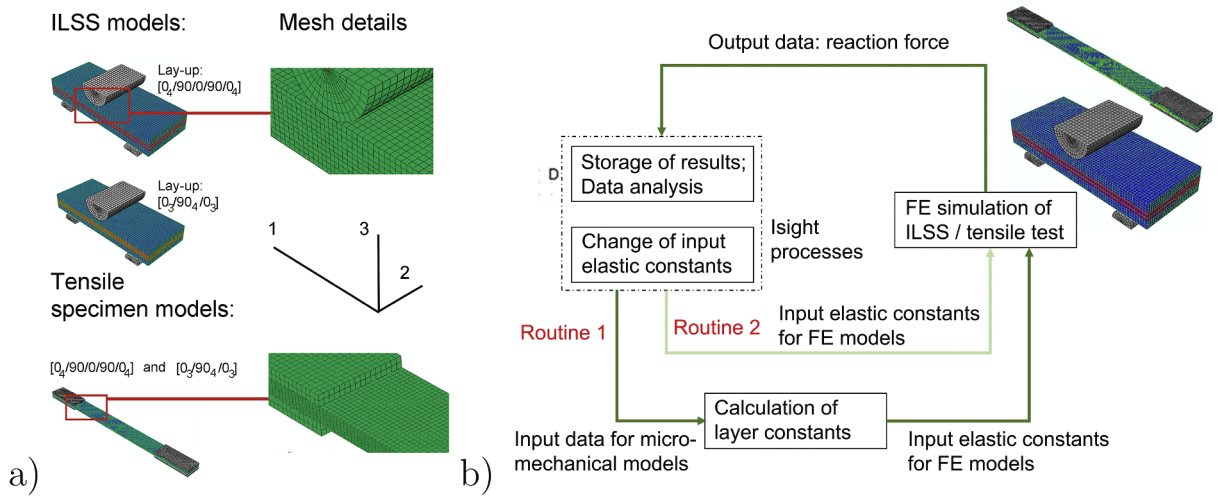

Fig. 1. FE models and process integration: a) FE models for ILSS and tensile tests; b) simulation routines for the layer level and micro level analysis.

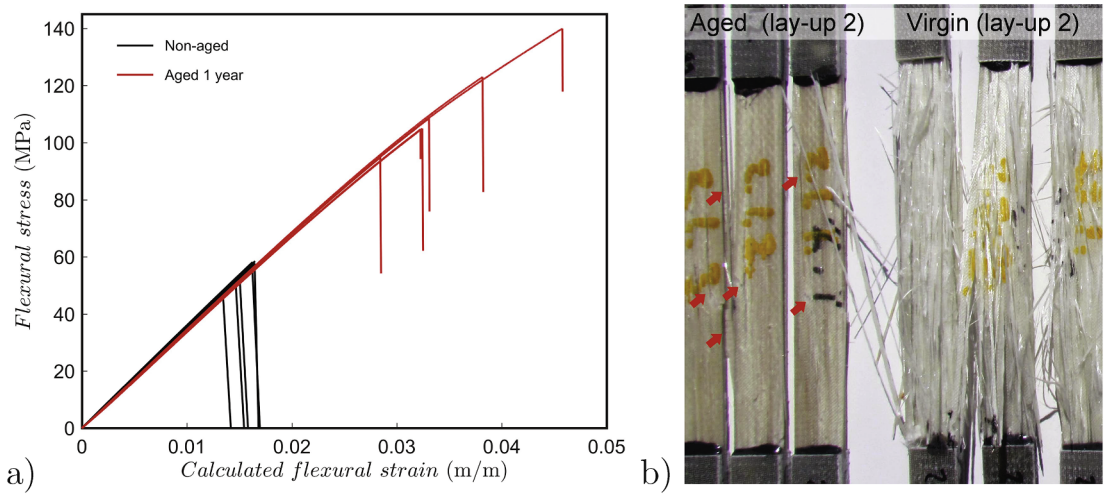

Fig. 2. a) Three-point bending results for the virgin and SAC conditioned matrix specimens; b) the overall failure mode change in tensile test composite specimens. The red arrows show the cracks in axial direction and delamination between layers of the aged laminate.

The layer material (engineering constants) was modelled using the well-known micromechanical models (all equations given in Appendix A), where the transverse and shear elastic constants were defined using the semi-empirical Halpin-Tsai parameter(s) [20]. These parameters are basically adjustable constants taking into account the uneven load transfer and stress distribution under transverse (or shear) loading. In reality, the uneven transverse stress field is affected by the fibre-matrix interphase, and the influence of the interphase can be thought to affect the Halpin-Tsai parameter value (parameter ξ_i, see Appendix) of transverse modulus (E_2) and shear moduli (G_{12} and G_{13}). Furthermore, since typically G_{12} and G_{13} do not match with G_{23}, a hypothesis can be set to consider that the Halpin-Tsai parameter is different when determining the modulus G_{23}, leading us to analyse two different values in this study (ξ_i and ξ_j, see Appendix A).

2.2.3. Quantitative aging in terms of Halpin-Tsai parameters

The potential impact of interfacial aging was studied by fitting the experimentally observed aging via the sole effect of the 'interfacial' Halpin-Tsai (ξ) parameters. The target was to consider if theoretical pure interfacial aging can explain the aging effects and, thereby, support any significant influence by the fibre-matrix interface upon aging. The study of the interfacial parameters was a two-step process. First, it was studied whether any realistic deviation of the values can result in the experimentally observed aging effects in tensile and ILSS tests (ξ values ranging from 0 to 100 through the simulation routine, any value above 100 being deduced false [20]). Second, exact values were fitted for a theoretical case where the aging is purely due to interfacial degradation. The tensile and ILSS test simulations with linearly decreasing ξ values were run until reaching the experimentally determined aging effect. The fitting was made presuming the effect of ξ the same on tensile and shear moduli ($\xi_i = \xi_j$) and also for a case where only shear modulus is affected ($\xi_i = 0$, $\xi_j \neq 0$).

3. Results and analysis

3.1. Matrix aging

The results of the three-point bending tests for the matrix are shown in Fig. 2. It can be seen that the stiffness went through a moderate (22%) but clearly observable aging: the average flexural modulus was determined to be 3.5 ± 0.1 GPa and 2.7 ± 0.1 GPa, for the virgin and SAC conditioned specimens, respectively. The ultimate strength, in turn, has increased significantly (109%) with the average values of 54 ± 5 MPa and 112 ± 16 MPa, for the virgin and SAC conditioned specimens, respectively. The proof stress of the conditioned specimens was determined (105 ± 13 MPa) whereas virgin specimens failed in a brittle manner reaching less than 0.05% plastic (non-linear) strain.

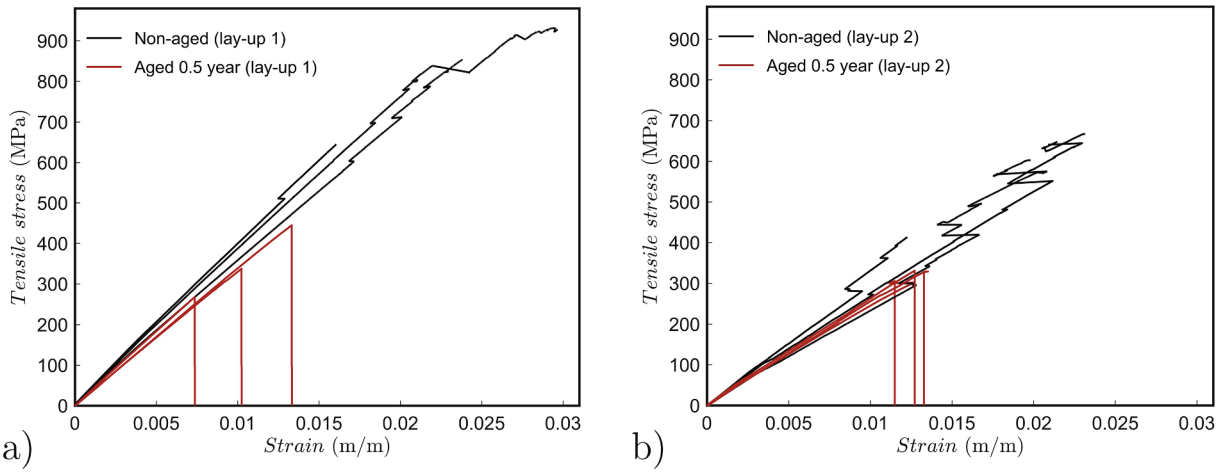

Fig. 3. Tensile test results for virgin and SAC conditioned specimens: a) lay-up 1 laminate specimens; b) lay-up 2 laminate specimens. Note that strain readings are not reliable after extensometer detachment (peaks).

Clearly, the pure matrix turned out to be stronger and more ductile after the one-year SAC conditioning.

3.2. Laminate aging

The determined weight fraction of fibres in the composite specimens was 76.5 ± 1.3%, which leads to a fibre volume fraction of V_f = 59.2%. No observable difference was noted between the virgin and aged samples.

The overall change in the failure mode of tensile specimens is shown in Fig. 2b and force-strain curves of the tensile tests are shown in Fig. 3. The overall failure mode was not observed largely changed when comparing those of both lay-ups. The laminate with the lay-up 1, with a dominating amount of axial fibres, has went through a 17% decrease in Young's modulus (41.7 ± 2.6 GPa compared to 34.7 ± 2.1 GPa) and an extensive 42% decrease in strength (602 ± 93 MPa compared to 346 ± 90 MPa) and also brittleness (proof stress could only be determined for the virgin laminate, at 263 ± 92 MPa). The results for the lay-up 2 (Fig. 3b) show that an increase in the transverse reinforcement led to only a nominal 5.6% decrease in Young's modulus (28.5 ± 3.3 GPa compared to 26.9 ± 2.5 GPa) and, indeed, to a 13% decrease in strength (320 ± 17 MPa compared to 283 ± 11 MPa) after the aging. Proof stress values could only be determined for the virgin laminate (187 ± 45 MPa), which indicates that the conditioning turned also the behavior of the laminate with the lay-up 2 into a brittle one. When considering the aging effects in the matrix (Fig. 2a), the results with both lay-ups suggest that either the fibres or the interfaces must have damaged due to the aging. Because the decrease in tensile Young's modulus was higher for the lay-up 1 and also because the amount of decrease was clearly higher than pure matrix aging would let anticipate (0.408 × 22% = 9%), the degradation of fibre stiffness is obvious.

The stress–strain curves of the ILSS tests are shown in Fig. 4. The lay-up 1 laminate, with a dominating amount of axial fibres, did not markedly degrade in terms of flexural stiffness (10.4 ± 3.6 GPa compared to 9.8 ± 2.2 GPa) but the ultimate flexural strength decreased 26% (433 ± 55 MPa compared to 321 ± 19 MPa).

The results for the lay-up 2 (Fig. 4b) show that an increase in the transverse reinforcement led to a significant decrease in stiffness within the conditioning (49%), according to the determined values of 14.3 ± 1.4 GPa and 7.3 ± 1.3 GPa, for the virgin and conditioned laminate, respectively. Likewise, the flexural strength was 34% lower for the conditioned specimens (387 ± 48 MPa compared to 287 ± 20 MPa). In general, when a laminate involves a dominating amount of transverse reinforcement, the behavior of the matrix and fibre matrix interface begin to govern the laminate mechanical response. The revealed fact, that the lay-up 2 experienced more severe decrease in flexural stiffness (as well as strength) than the lay-up 1, indicates aging of the fibre matrix interface. The effect of fibre matrix interfaces is difficult to clearly point out based on the macro scale test results and, hence, characterisation of micro scale failure modes and numerical analyses are necessary.

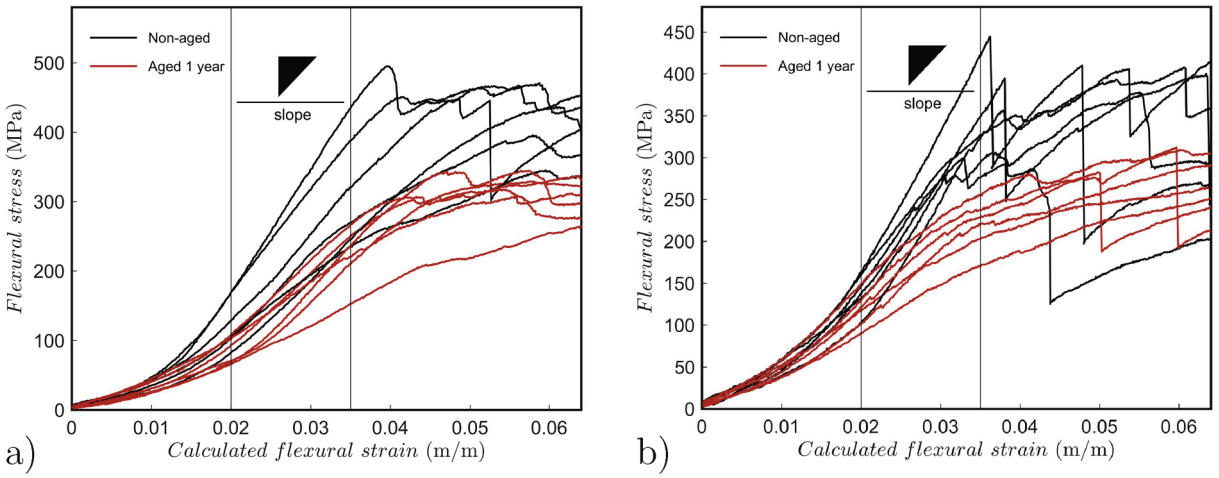

Fig. 4. ILSS test results for the virgin and SAC conditioned specimens: a) the lay-up 1 laminate specimens; b) the lay-up 2 laminate specimens.

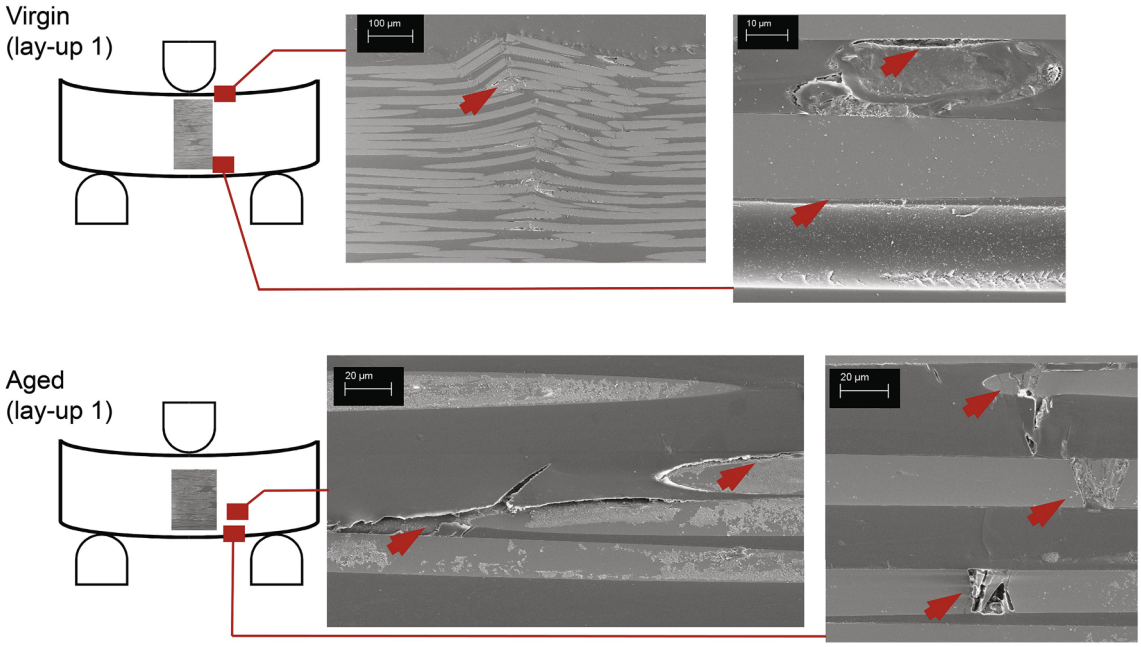

Fig. 5. Failure modes in ILSS tests for virgin and SAC conditioned specimens (lay-up 1 laminate specimens).

3.3. Failure modes

The failure modes observed in the ILSS specimens' cross-sections are shown in Figs. 5 and 6. All the cross-sections were cut along the long-axis of the specimen. The macroscopic failure mode in the specimens with the lay-up 1 was mostly interlaminar between the filament wound axial layers independent of the condition (Fig. 5). Especially for the virgin laminate, ILSS tests resulted in local fibre buckling on the upper surface with compressive loading. Distinctively, the effect of aging was shown by shattered axial fibres on the lower part of the specimen where tensile load prevails—this clearly suggests degraded fibre properties since the matrix strength was improved. The interfacial damage tended to occur more on the matrix side and could suggest a change in the fibre matrix interfacial strength.

The increase in transverse reinforcement at the neutral axis of the specimen (i.e. lay-up 2, Fig. 6) expectedly led to a change in the ILSS failure mode. The presumed failure occurred amidst the neutral axis due to shear load and propagated through the transverse layers and further towards the specimen free end. For the lay-up 2, the aging did not observably affect the micro scale failure mode. However, the significantly decreased flexural stiffness and strength values suggest that the composite's shear modulus and further the fibre-matrix interfacial strength decreased because of aging. It should be noted that a post-test analysis of the failure modes does not produce clear information about the changes in *stiffness*.

3.4. Sensitivity analysis

In order to separately study the effects of fibre degradation and fibre

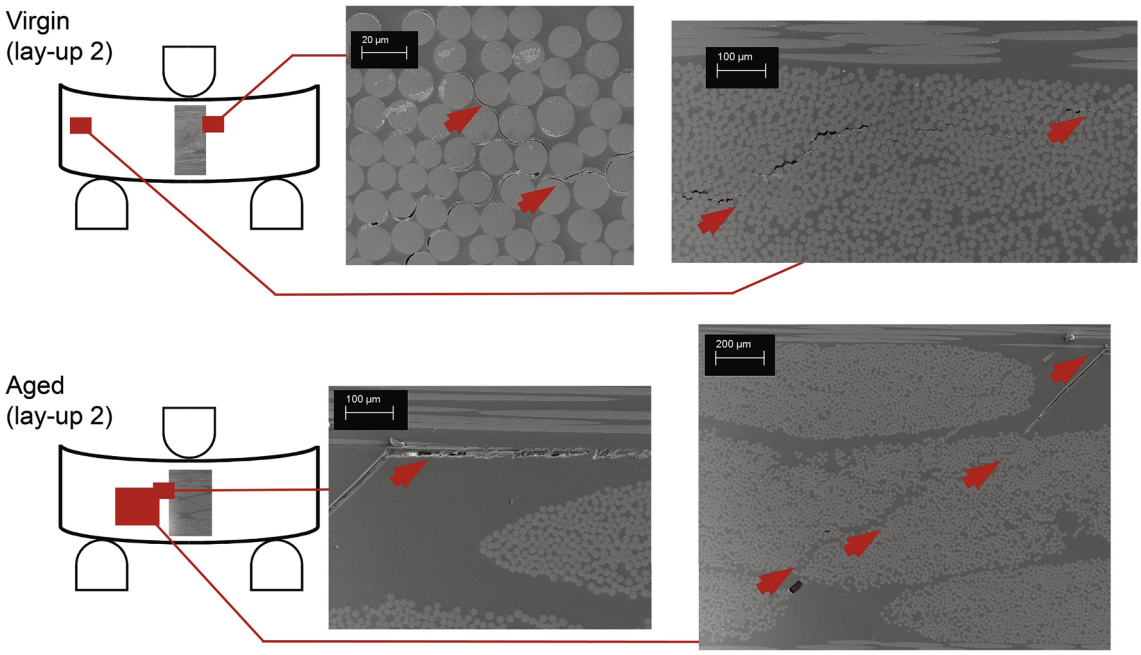

Fig. 6. Failure modes in ILSS tests for virgin and SAC conditioned specimens (lay-up 2 laminate specimens).

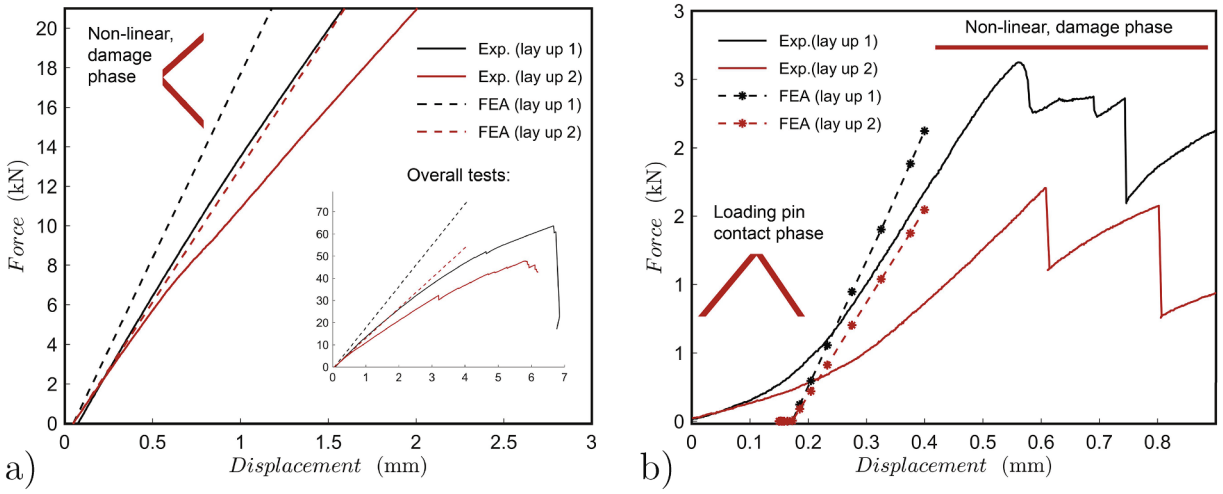

Fig. 7. Comparisons between the FE models and experiments: a) force–displacement curves for the tensile testing; b) force–displacement curves for the ILSS testing.

matrix interface, numerical sensitivity analyses were run. First, the validity of the models was studied. For both test types, the FE models were observed slightly stiffer compared to experiments, as is typical. For the linear behavior range (as defined for tensile and flexural modulus here), good correlation was found for the virgin material properties and for both lay-ups (Fig. 7) giving a solid basis for the simulations of aging effects.

The sensitivity analyses were carried out by surveying the effect of different combinations of engineering constants of the single layer material model. The results for the tensile test simulation and the two lay-ups are shown in Fig. 8. The analysis for the tensile test naturally highlights the governing influence of axial modulus (E_1) on the specimen stiffness, noting that both lay-ups involve a dominant amount of axially oriented reinforcement layers. When the number of transverse layers is increased (for the lay-up 2), the influence of transverse modulus (E_2) starts to play a role.

The simulation results for the ILSS tests on the layer scale are shown in Fig. 9. It can be seen that, in addition to the dominating effect of E_1, the stiffness in the thickness direction (E_3) affects the simulation results due to the deformation by the out-of-plane force (loading pin). The sensitivity of the results on the shear moduli G_{13} and G_{23} is observable but low for the lay-ups in this study. The influence of G_{13} is clear because of the high shear load upon an ILSS test and the dominating amount of 0° layers. Because of the 90° layers, also G_{23} has an effect. The load transfer between different directions (Poisson's effects) does not observably affect the aging-tension or aging-bending response.

In the second numerical analysis phase, sensitivity analyses were run with an additional routine to implement the micromechanical models for determining the layer model's engineering constants. The results (Figs. 10 and 11) show that the fibre stiffness (E_f) has a dominating effect on the load–displacement response for both tensile test and ILSS test—agreeing directly with the engineering constant based analysis (a dominating effect by E_1). The difference between the tensile test and ILSS test is that the sensitivity to the values of other factors than fibre modulus is higher for the ILSS test. For the tensile test, it is not probable that stiffness degradation could be explained by other phenomena than fibre degradation (laminate behavior is not sensitive to other than fibre stiffness, see Fig. 10). On the other hand, the observed insensitivity means that the degradation of other properties, such as interfacial micro scale strength, is essentially not shown in the tensile response.

Due to the strong loading of interfaces (shearing of transverse layers at neutral plane) during ILSS testing, it is probable that a change in the matrix and interface dominated properties reveals itself. The simulation results on ILSS (Fig. 11) show that the flexural stiffness is highly sensitive to the changes in matrix modulus as well as in the interfacial parameters (Halpin-Tsai parameters for moduli E_2, E_3, G_{13}, G_{12}). Interestingly, the sensitivity to interfacial parameters (either ξ_i, or ξ_j for shear moduli) is even higher than the sensitivity to the matrix modulus for both lay-ups studied.

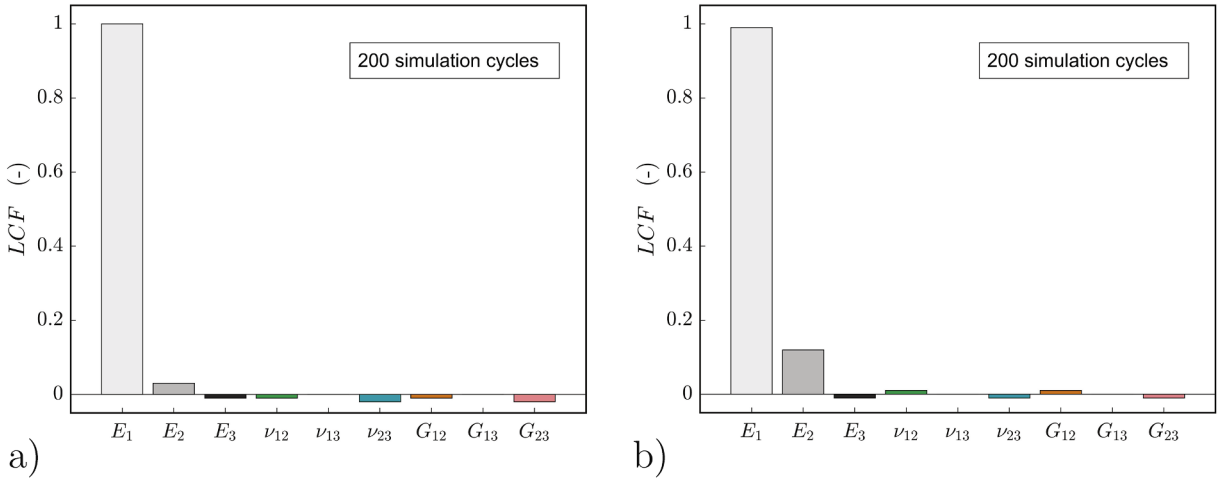

Fig. 8. Sensitivity analysis results on the layer model and regarding the laminate tensile stiffness: a) for the lay-up 1; b) for the lay-up 2.

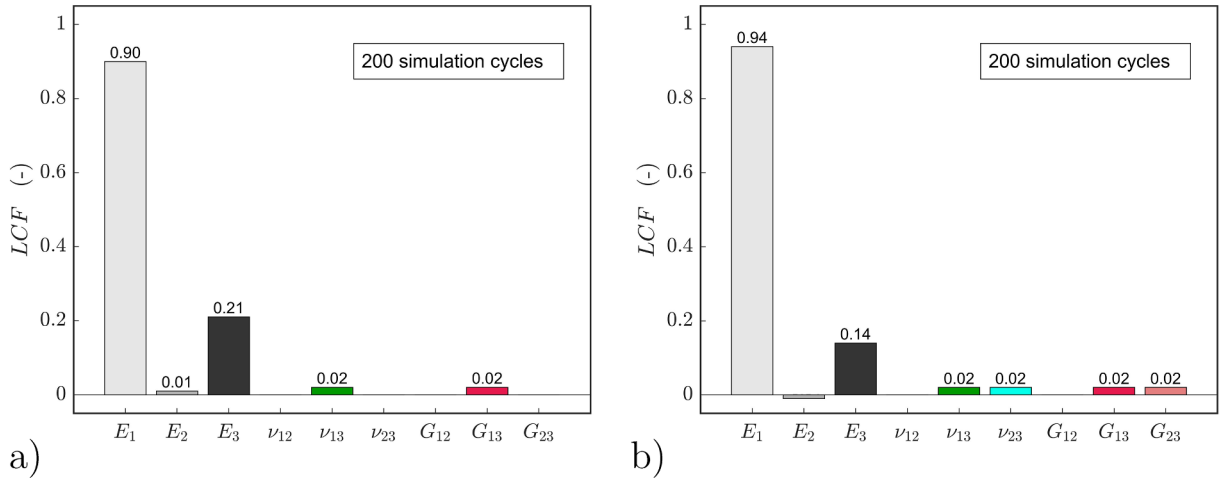

Fig. 9. Sensitivity analysis results on the layer model and regarding the laminate flexural stiffness during an ILSS test: a) for the lay-up 1; b) for the lay-up 2.

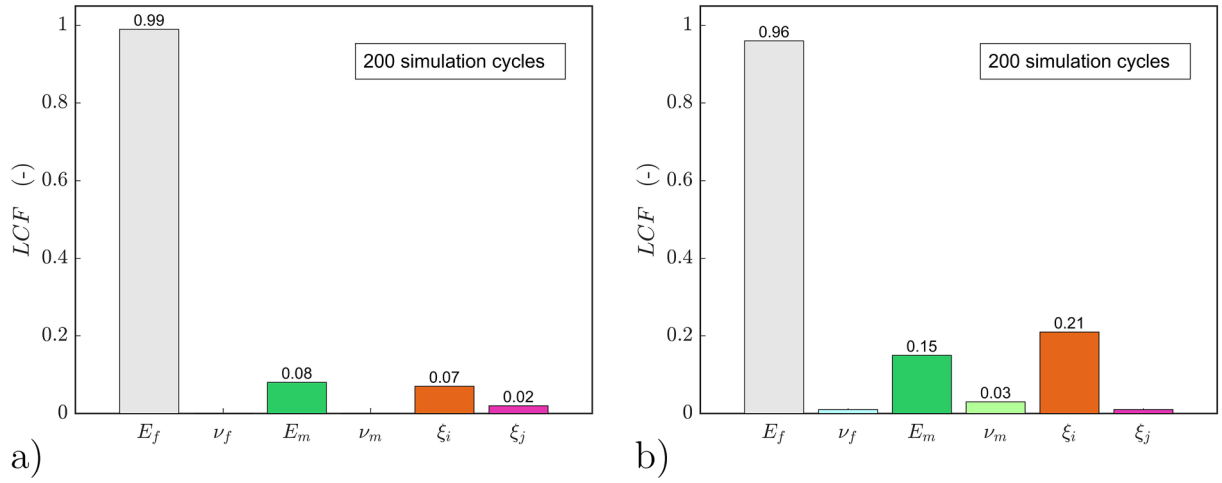

Fig. 10. Sensitivity analysis results on the micromechanics scale and regarding the laminate stiffness during an tensile test: a) for the lay-up 1; b) for the lay-up 2.

3.5. Model parameters for GFRP aging

As a final analysis step, it is needed to study whether the experimentally observed degradation could be explained quantitatively by interfacial degradation or not. The target change in the flexural stiffness was determined according to the test results from experiments (see Table 2). Since the effect of ξ is to monotonically increase the value of both Young's moduli and shear moduli, as shown in Fig. 12, the reference point of simulation was set to the lowest stiffness, i.e., when $\xi = 0$. Then, the target force as an acceptance criterion was set based on the ratio of experimental values of virgin specimens to those of aged specimens.

The results of the iteration, in Tables 3 and 4, show that the degradation observed in tensile tests can only be covered by the interfacial effect on transverse modulus E_2, via ξ_i (see Eq. (A.2) and Fig. 8). However, it is needed to cover almost the entire range (88%) of the ξ_i values—here the maximum value per typical theories is presumed two [20]. In contrast, degradation of the flexural modulus upon ILSS tests can be readily covered in the case of the lay-up 1. However, since the ILSS test is only sensitive to E_3 via ξ_i and there is no difference in the sensitivity to shear moduli between the lay-ups, the simulated aging effect is merely originating from the degradation of matrix under compression (under the loading pin). This effect and the relation to a change in the value of ξ_i is because of the assumption that $E_2 = E_3$. It is interesting to see that the target degradation for lay-up 2 cannot be reached with any reasonable value of ξ (0…100).

4. Discussion

In the current literature, the aging of GFRP laminates subjected to hygro-thermal conditioning as well as due to various chemicals has been demonstrated for different matrix polymers. In detail, because of the diffusion of constituent ions of H_2SO_4, the effect of pure moisture, or its dissociated components OH^- and H_3O^+ on the matrix and fibre matrix interface [21,22] oppose the effects solely by acid molecules and sulfurous ions [23]. Due to the sheer size of the molecules, the penetration and effects by moisture are typically beyond those of acid [24]. The Mori–Tanaka solutions and the modified Benveniste solutions have been used to reveal the separate aging effects in 2D arrays of fibres and matrix. Fisher and Brinson [25] studied the effect of viscoelastic interphases on shear moduli and showed that the interphase is not likely to affect the aging effect in terms of (aging) time-shift rates. Recently, simulations using representative volume elements (RVEs) have been used to understand the separate effects of matrix, fibre and fibre matrix-related interphase. Rocha et al. [26] simulated 2D arrays accounting for different RVE sizes and interphase thicknesses to understand the overall diffusion in fibrous composite materials—they concluded that the interphase tends to enable better fit with experiments when orthotropic interfacial diffusion is accounted for.

Here, the experimental results for the tensile testing and ILSS testing indicated a clear, expected decrease in the tensile and flexural stiffness. The numerical sensitivity analysis revealed that the observed

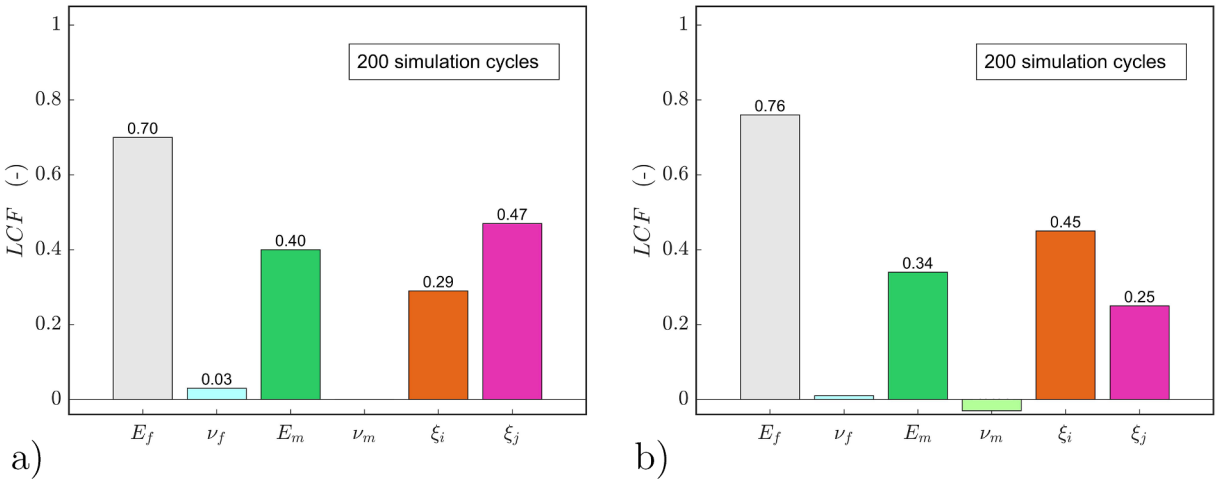

Fig. 11. Sensitivity analysis results on the micromechanics scale and regarding the laminate flexural stiffness during an ILSS test: a) for the lay-up 1; b) for the lay-up 2.

Table 2
Simulation targets to fit the ξ parameter values in order to reach experimentally observed degradation.

Lay-up	Experiment	Virgin stiffness (Exp. mean)	Degraded stiffness (Exp. mean)	Ratio
1	tensile	41.67	34.68	1.20
1	ILSS	10.44	9.79	1.07
2	tensile	28.50	26.90	1.06
2	ILSS	14.31	7.28	1.97

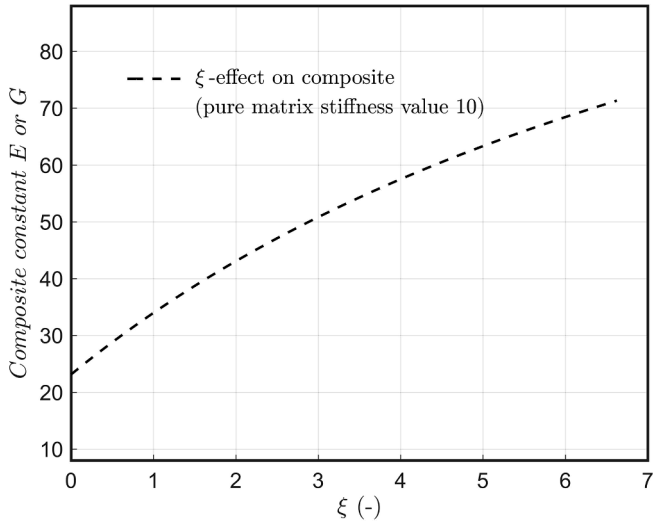

Fig. 12. The effect of ξ parameter on modulus values of composite material (V_f = 60%, E_f/E_m = 24.2).

Table 3
Simulation-fitted ξ parameter values for the tensile tests.

Lay-up	Simulated force, $\xi = 0$	Target force	Case $\xi_i = \xi_j \neq 0$	Case $\xi_i = 0$, $\xi_j \neq 0$
1	29545.1 N	35495 N	ξ = 100, failed	ξ = 100, failed
2	21232.1 N	22501 N	ξ = 1.76, 22501 N	ξ = 100, failed

degradation can only be due to deterioration of layer Young's moduli—only minor influence is accommodated through changes in shear deformation or Poisson's effect. The well-known micromechanical models determining the layer properties in turn showed that the tensile stiffness for either of the lay-ups can not be produced by realistic matrix aging or changes at fibre matrix interfaces but only by the aging of fibres. However, presuming that Halpin-Tsai parameters cover interfacial effects, it was shown that a typical value range of the parameters can solely produce the flexural stiffness deterioration observed in ILSS tests. Therefore, since interfacial effects are not shown by the tensile tests (Fig. 8) and because the stiffness deterioration was more pronounced for the lay-up 2, interfacial aging by the SAC immersion is highly probable to exist in this study. However, it influences laminate behavior via changing the layer-wise Young's modulus in the thickness direction (E_3, see Fig. 9) and under local compressive loading.

It is not known how exactly interfacial aging could affect composite transverse stiffness. Basically, interfacial detachment of matrix from the fibres could occur already over the ('linear') low-strain loading regime of an aged laminate. Alternatively, in the event of non-mechanical but chemical destruction of interfacial bonds [27] during immersion, gradual sliding or opening of micro cracks upon external loading could lead to lower overall stiffness of the composite. This type of mechanism could be the reason behind the mostly non-linear stress–strain response during the ILSS tests (Fig. 4), and is also supported by the SEM imaging (e.g., Fig. 5). To verify the micro scale mechanisms at interfaces, fracture mechanics modelling of fibre matrix interfaces would be needed along with proper micro scale experiments. Zhang et al. [10] studied thermo-oxidative aging using RVEs on the length scale of tows and found out that interfacial damage significantly affects the compressive stiffness in transverse direction (≈ 26% of the modulus deterioration). The FE modelling by Zhang et al. included a cohesive zone model of the carbon fibre matrix interface, thus, was theoretically able to include the fibre matrix bond degradation in the RVE. However, for a glass fibre-reinforced composite, fibres cannot be presumed inert making it challenging to model single-fibre aging or to compare the results with the study by Zhang et al.

5. Conclusions

This work aimed to reveal the sources of aging on GFRP laminate stiffness when subjected to sulfuric acid–water immersion (90 °C, 15 bar). Tensile and interlaminar flexural tests were carried out for two different laminate lay-ups to emphasise fibre and matrix dominated behavior. The two tests were simulated by using finite element models for both lay-ups and material models on two different length scales. Several hundreds of simulation cycles were automatically run to determine statistical sensitivities of elastic constants per material model. Based on the results, we conclude that the SAC immersion leads to the

Table 4
Simulation-fitted ξ parameter values for the ILSS tests.

Lay-up	Simulated force, $\xi = 0$	Target force	Case $\xi_i = \xi_j \neq 0$	Case $\xi_i = 0$, $\xi_j \neq 0$
1	1814 N	1935 N	$\xi = 0.28$, 1935.5 N	$\xi = 0.46$, 1934.4 N
2	1358 N	2669 N	$\xi = 100$, failed	$\xi = 100$, failed

following degradation and origin:

- the flexural modulus of the epoxy-vinylester matrix decreased by 22% but the ultimate strength increased by 109% after one-year immersion;
- the tensile Young's modulus of the GFRP cross-ply laminate decreased by 5.6–17% and the ultimate strength by 13–42% after six months of conditioning;
- the deterioration of tensile properties is caused by lower E_1 and E_2 on the layer length scale;
- the flexural stiffness of the composite was 6–49% lower and the flexural strength 26–34% lower after six months of conditioning;
- the deterioration of flexural stiffness is caused by lower E_1 and E_3 where E_3 is affected by fibre matrix interfaces via Halpin-Tsai parameters;
- on the micro scale, the aging is mainly subjected to the fibres and the aging of interfaces cannot be excluded as regards the linear elastic response within bending.

Acknowledgement

This investigation has got support from Tekes and Business Finland in the form of granted funding related to projects 'FIMECC LIGHT' and 'FIMECC HYBRIDS'. The authors are grateful to Muovityö Hiltunen Oy for collaboration.

Data availability

The raw data required to reproduce part of the experimental results are available for download (doi: 10.17632/7yz27z8vbx.1).

Appendix A. Micromechanical model with interphase related parameters

Given that axial fibre stiffness (E_f) and composite's volume fraction (V_f) are known, the axial (0°) modulus of an unidirectionally reinforced layer is calculated by using the rule of mixtures:

$$E_1 = V_f E_f + (1 - V_f) E_m, \tag{A.1}$$

where voids are not taken into account as they are not explicitly modelled, and E_m is the Young's modulus of the matrix (epoxy-vinylester matrix here). For the transverse Young's modulus, the well-known (see introduction e.g. in [20]) Halpin-Tsai relationship yields:

$$E_2 = \frac{E_m(1 + \xi_i \eta V_f)}{1 - \eta V_f}, \tag{A.2}$$

where η and ξ are parameters to account for a set factors, such as interfaces and interphases around the fibers, that affect the transverse load transfer through the reinforced medium. The parameter η is defined:

$$\eta = \frac{\frac{E_f}{E_m} - 1}{\frac{E_f}{E_m} + \xi_i}, \tag{A.3}$$

where ξ is typically considered as an adjustable parameter. Here, it is presumed that $E_2 = E_3$. Similarly as for E_2, an equation can be derived for the in-plane shear modulus:

$$G_{12} = \frac{G_m(1 + \xi_j \eta V_f)}{1 - \eta V_f}, \tag{A.4}$$

where G_m is the (known) shear modulus of matrix, and η is given by Eq. (A.3) for $j = i$ and $E \rightarrow G$. Furthermore, it is presumed that $G_{12} = G_{13}$. However, the value of G_{23} typically differs from those of the two other ply shear moduli [20], and it can be derived for a transversely isotropic layer (in addition to relation $\nu_{12}/E_1 = \nu_{21}/E_2$):

$$G_{23} = \frac{E_2}{2(1 + \nu_{23})}. \tag{A.5}$$

The modelling of ply Poisson's ratios requires further consideration. For axial direction, an equal strain approximation is rather accurate, so that simple rule of mixtures can be applied for the in-plane Poisson's ratio ν_{12}:

$$\nu_{12} = V_f \nu_f + (1 - V_f) \nu_m, \tag{A.6}$$

where the Poisson's ratio of fibre (ν_f) and matrix (ν_m) are presumed as known constants. For a finite element application, it assumed that $\nu_{12} = \nu_{21}$ (not true in detail) and that $\nu_{12} = \nu_{13}$. Then, the third direction Poisson's effect is derived based on the overall volume change ($\Delta = \varepsilon_1 + \varepsilon_2 + \varepsilon_3 = \sigma_{hp}/K$) due to the hydrostatic stress (σ_{hp}):

$$\nu_{23} = 1 - \nu_{21} - \frac{E_2}{3K}, \tag{A.7}$$

where K is the bulk modulus. An approximation of the composite bulk modulus, according to the equal stress assumption, reads as follows:

$$K = \frac{\sigma_{hp}}{\Delta} = \left(\frac{V_f}{K_f} + \frac{1 - V_f}{K_m} \right)^{-1}. \tag{A.8}$$

For the fibre, being anisotropic in reality, the bulk modulus is estimated here as follows:

$$K_f = \frac{E_f}{3(1 - 2\nu_f)}. \tag{A.9}$$

Bulk modulus for matrix naturally follows the isotropic formulation (such as Eq. (A.9)).

References

[1] Myers T, Kytömaa H, Smith T. Environmental stress corrosion cracking of fiberglass: Lessons learned from failures in the chemical industry. J Hazard Mater 2007;142(3):695–704.
[2] Lindgren M, Bergman G, Kakkonen M, Lehtonen M, Jokinen J, Wallin M, et al. Failure analysis of a leaching reactor made of glass-fiber reinforced plastic. Eng Failure Anal 2015;60(1):117–36.
[3] Tsai S. Composite Design. 4th ed Dayton: Think Composites; 1988.
[4] Zhang T, Li S, Chang F, Shi X, Li L. An experimental and numerical analysis for stiffened composite panel subjected to shear loading in hygrothermal environment. Compos Struct 2016;138(1):107–15.
[5] Oliveira B, Creus G. An analytical-numerical framework for the study of ageing in fibre reinforced polymer composites. Compos Struct 2004;65(1):443–57.
[6] Kanerva M, Sarlin E, Hoikkanen M, Rämö K, Saarela O, Vuorinen J. Interface modification of glass fibre-polyester composite-composite joints using peel plies. Int J Adhes Adhes 2015;59(1):40–52.
[7] Davies P, Baley C, Loaec H, Grohens Y. Interlaminar tests for marine applications. Evaluation of the influence of peel plies and fabrication delays. Appl Compos Mat 2005;12(5):293–307.
[8] Jones R, Stewart J. The kinetics of corrosion of E-glass fibres in sulphuric acid. J Non-Cryst Solids 2010;356(1):2433–6.
[9] Jones R. Chemical corrosion of E-glass fibers in oxalic and other organic acids. J Am Ceram Soc 2006;89(1):20–3.
[10] Zhang M, Sun B, Gu B. Meso-structure ageing mechanism of 3-D braided composite's compressive behaviors under accelerated thermo-oxidative ageing environment. Mech Mater 2017;115(1):47–63.
[11] Mlyniec A, Korta J, Uhl T. Structurally based constitutive model of epoxy adhesives incorporating the influence of post-curing and thermolysis. Compos Part B Eng 2016;86(1):160–7.
[12] Sarlin E, Saarimäki M, Sironen R, Lindgren M, Siljander S, Kanerva M, et al. Erosive wear of filled vinylester composites in water and acidic media at elevated temperature. Wear 2017;390–391:84–92.
[13] Sarlin E, Sironen R, Pärnänen T, Lindgren M, Kanerva M, Vuorinen J. The effect of matrix type on ageing of thick vinyl ester glass-fibre-reinforced laminates. Compos Struct 2017;168(1):840–50.
[14] Gustafson P, Waas A. The influence of adhesive constitutive parameters in cohesive zone finite element models of adhesively bonded joints. Int J Solids Struct 2009;46(1):2201–15.
[15] Jokinen J, Kanerva M. Sensitivity analysis for simulated testing of composites: mapping via Isight and Abaqus. J Structural Mech 2017;50(3):191–7.
[16] Posio J. Interlaminar shear strength testing of non-unidirectionally reinforced composites M.Sc. thesis Finland: Aalto University; 2016.
[17] Derakane 441-400 epoxy vinyl ester resin. Technical data sheet, Ashland Composites; 2011.
[18] Direct roving 386 for wilament winding, pultrusion and weaving. Technical data sheet, Jushi; 2011.
[19] Oguni K, Tan C, Ravichandran G. Failure mode transition in unidirectional E-glass/vinylester composites under multiaxial compression. J Compos Mater 2000;34:2081–97.
[20] Hull D, Clyne T. An introduction to composite materials; chap. Elastic deformation of long-fibre composites. Cambridge University Press; 1996. p. 60–77.
[21] Fraga A, Alvarez V, Vázquez A. Relationship between dynamic mechanical properties and water absorption of unsaturated polyester and vinyl ester glass fiber composites. J Compos Mater 2003;37(17):1553–74.
[22] Zhou J, Lucas J. Hygrothermal effects of epoxy resin. Part I the nature of water in epoxy. Polymer 1999;40(1):5505–12.
[23] Cabral-Fonseca S, Correia J, Rodrigues M, Branco F. Artificial accelerated ageing of GFRP pultruded profiles made of polyester and vinylester resins: characterisation of physical-chemical and mechanical damage. Strain 2012;48(1):162–73.
[24] Regester R. Behavior of fiber reinforced plastic materials in chemical service. Corrosion Nace 1969;25:157–67.
[25] Fisher F, Brinson L. Viscoelastic interphases in polymer–matrix composites: theoretical models and finite-element analysis. Compos Sci Technol 2001;61(1):731–48.
[26] Rocha I, Raijmaekers S, van der Meer F, Nijssen R, Fischer H, Sluys L. Combined experimental/numerical investigation of directional moisture diffusion in glass/epoxy composites. Compos Sci Technol 2017;151(1):16–24.
[27] Hodzic A, Kim J, Stachurski Z. Nano-indentation and nano-scratch of polymer/glass interfaces. II: model of interphases in water aged composite materials. Polymer 2001;42(1):5701–10.